J Mol Model (2016) 22: 193
DOI 10.1007/s00894-016-3058-1

ORIGINAL PAPER

Reexamination of structures, stabilities, and electronic properties of holmium-doped silicon clusters $HoSi_n$ (n = 12–20)

Liyuan Hou[1] · **Jucai Yang**[1,2] · **Yuming Liu**[3]

Received: 13 March 2016 / Accepted: 3 July 2016 / Published online: 28 July 2016

Abstract The total energies, growth patterns, equilibrium geometries, relative stabilities, hardnesses, intramolecular charge transfer, and magnetic moments of $HoSi_n$ (n = 12–20) clusters have been reexamined theoretically using two different density functional schemes in combination with relativistic small-core Stuttgart effective core potentials (ECP28MWB) for the Ho atoms. The results show that when n = 12–15, the most stable structures are predicted to be exohedral frameworks with a quartet ground state, but when n = 16–20, they are predicted to be endohedral frameworks with a sextuplet ground state. These trend in stability across the clusters (gauged from their dissociation energies) was found to be approximately the same regardless of the DFT scheme used in the calculations, with $HoSi_{13}$, $HoSi_{16}$, $HoSi_{18}$, and $HoSi_{20}$ calculated to be more stable than the other clusters. The results obtained for cluster hardness indicated that doping the Ho atom into Si_{13} and Si_{16} leads to the most stable $HoSi_n$ clusters, while doping Ho into the other Si_n clusters increases the photochemical sensitivity of the cluster. Analyses of intracluster charge transfer and magnetic moments revealed that charge always shifts from the Ho atom to the Si_n cluster during the creation of exohedral $HoSi_n$ (n = 12–15) structures. However, the direction of charge transfer is reversed during the creation of endohedral $HoSi_n$ (n = 16–20) structures, which implies that Ho acts as an electron acceptor when it is encapsulated in the Si_n cage. Furthermore, when the most stable exohedral $HoSi_n$ (n = 12–15) structures are generated, the 4*f* electrons of Ho are virtually unchanged and barely participate in intracluster bonding. However, in the most stable endohedral $HoSi_n$ (n = 16–20) frameworks, a 4*f* electron does participate in bonding. It does this by transferring to the 5*d* orbital, which hybridizes with the 6*s* and 6*p* orbitals and then interacts with Si valence *sp* orbitals. Meanwhile, the total magnetic moments of the $HoSi_n$ (n = 16–20) clusters are considerably higher than those of $HoSi_n$ (n = 12–15). Interestingly, the endohedral $HoSi_{16}$ and $HoSi_{20}$ clusters can be viewed as the most suitable building blocks for novel high-density magnetic storage nanomaterials and for novel optical and optoelectronic photosensitive nanomaterials, respectively.

Keywords $HoSi_n$ · Magnetic moment · Relative stability · Hardness · Charge transfer

Introduction

In the past few years, extensive theoretical and experimental research has been performed on silicon clusters due to their distinctive chemical structures and bonding, as well as their wide range of applications in the microelectronics industry [1–14]. The ground-state structures of small (Si_{2-7}) clusters have been determined using theoretical [1–3] and experimental [10–14] methods. Especially for large molecular clusters, it was found that the ground-state geometry can depend upon the method and basis set used to calculate it. Many calculations [4–8] have indicated that the most stable structures for medium-sized silicon clusters with less than 27 Si atoms can be categorized into two types: one is TTP (a tricapped trigonal prism structure); the other

✉ Jucai Yang
yangjc@imut.edu.cn

[1] School of Energy and Power Engineering, Inner Mongolia University of Technology, Hohhot 010051, People's Republic of China

[2] Inner Mongolia Key Laboratory of Theoretical and Computational Chemistry Simulation, Hohhot 010051, People's Republic of China

[3] School of Chemical Engineering, Inner Mongolia University of Technology, Hohhot 010051, People's Republic of China

is SS (a structure containing a sixfold-puckered hexagonal ring and six-atom tetragonal bipyramid).

In recent years, rare earth metal (REM)-doped silicon clusters have attracted increasing attention because they can be used to miniaturize electronic equipment and they can be employed as self-assembled materials with many unusual optical, electronic, and magnetic properties [15–20]. In particular, doping lanthanide (Ln) atoms into a silicon cluster is regarded as a promising way to modify the magnetic properties of silicon. Since the 4*f* electrons in some REMs such as Sm and Eu barely participate in the bonding in their corresponding $REMSi_n$ clusters, these REM atoms can retain their atomic magnetic moments when they are incorporated into $REMSi_n$ clusters. On the other hand, in other REM atoms such as Pr, the 4*f* electrons do participate in the bonding in the $REMSi_n$ cluster; here, a 4*f* electron is transferred to the 5*d* orbital and becomes involved in bonding. Nevertheless, the total magnetic moment of the REM atom in $REMSi_n$ differs little from that of the isolated REM atom. However, when late-REM atoms are included in silicon clusters, such as the $HoSi_{16–20}$ clusters studied in this paper, the total magnetic moment increases when a 4*f* electron is transferred to the 5*d* orbital. REM atoms differ from transition metal (TM) atoms in this regard; upon doping TM atoms into semiconductor clusters such as Si_n and Ge_n, the magnetic moment can be quenched [21, 22]. In addition to the magnetic moment, the implantation of REM atoms into silicon clusters can result in clusters with excellent optical properties; for example, doping an erbium atom into a silicon microcrystal yields a silicon-based optical source [23].

Although studies on REM-doped silicon clusters are still relatively rare, interest in their potential applications has stimulated a fair amount of research interest in these clusters over the past few years. Nakajima and co-workers [15, 24] were the first to investigate $TbSi_n^-$, $HoSi_n^-$, and $LuSi_n^-$ ($6 \leq n \leq 20$) clusters experimentally using PES (photoelectron spectra) and a chemical probe. Their results suggested that when a Ho atom is encapsulated in a Si cage, the cage is incomplete when the number of Si atoms is less than 16. Bowen and co-workers [16] then explored the properties of $HoSi_n^-$, $PrSi_n^-$, $GdSi_n^-$, $SmSi_n^-$, $EuSi_n^-$, and $YbSi_n^-$ ($3 \leq n \leq 13$) using PES. These REM-doped silicon clusters were categorized into two or three groups based on their appearance. In light of our experience [25–27], we believe that dividing the clusters into two groups is more reasonable than dividing them into three groups. Group A contains $EuSi_n^-$, $YbSi_n^-$, and $SmSi_n^-$, in which the 4*f* electrons of the REM atom barely participate in bonding. Group B contains $HoSi_n^-$, $GdSi_n^-$, and $PrSi_n^-$, in which the 4*f* electrons of the REM atom do participate in bonding. Spurred on by these experimental results, some theoretical studies have been carried out on REM-doped Si_n species [28–37].

Recently, Zhao et al. [38] investigated the geometries and properties of $HoSi_n$ ($n = 10–20$) clusters theoretically using X3LYP functionals in combination with large-core potentials (ECP56MHF) for Ho atoms and 6-31G basis sets for Si atoms. The use of large-core (4*f*-in-core) basis sets for Ho atoms is unreasonable because the main difference between the Ln elements is that they all contain different numbers of electrons in their 4*f* shells. At the same time, the 4*f* electrons are valence electrons that can participate in bonding. Thus, 4*f*-in-core basis sets cannot accurately reflect the interaction between the Ln atom and the surrounding atoms, especially in a system with strongly interactions. Even if the 4*f* electrons are not involved in bonding, the electron configuration and the shapes of the 4*f* orbitals will be affected, so the electronic state will also be influenced. However, the ground-state structure is ultimately determined by the electronic state, and sometimes the energy differences between various electronic states are significant, so it is necessary to use small-core (4*f*-in-valence) basis sets to calculate structures and properties. We therefore reexamined the total energies, structures, and electron properties such as the growth pattern, structure, hardness, population analysis, and magnetic moment of each $HoSi_n$ ($n = 12–20$) cluster using two carefully selected density functionals in combination with relativistic small-core potential (ECP) basis sets for the Ho atom and cc-pVDZ for the Si atom in order to probe their unusual size-dependent electronic properties as well as the critical size of a silicon cluster encapsulating a Ho atom. This information should help to guide the development of new cluster-assembled materials. Two different functionals were utilized in this work to check whether the results of the theoretical determination of the most stable structures were dependent on the functional used in the calculations, as this phenomenon has been shown to occur for Si_n species [7, 8].

Computational details

The calculations were performed using the Gaussian 09 software at the DFT level with the PBE0 [39] and B3LYP [40, 41] functionals in combination with the cc-pVDZ basis set [42] for Si atoms and relativistic small-core potentials (ECP28MWB) [43] (named SEG/ECP) for Ho atoms [44]. All stationary-point isomers of the $HoSi_n$ ($n = 12–20$) clusters were identified by calculating their vibrational frequencies with the two schemes. The optimized structures were obtained as local minima and ZPVE (zero-point vibrational energy) corrections were performed.

To search for the ground-state structures, a large number of isomers were studied in order to ensure that we did not overlook the lowest-energy isomers. At small cluster sizes, this approach is feasible. However, as the cluster size increases it becomes more difficult. There are two main reasons for this: one is the increase in the number of low-lying isomers as cluster size increases; the other is that large clusters cannot be efficiently and accurately optimized. In spite of this, the

rules derived from calculations of smaller REM-doped Si_n clusters can be applied to calculate medium and large $REMSi_n$ clusters. Cao et al. [33] performed a global search using a genetic algorithm (GA) to study $LuSi_n$ ($n = 1–12$) clusters, and concluded that the most stable structures were those obtained by replacing a Si atom in the lowest-energy structure of the pure Si_{n+1} cluster with a Lu atom (a "substitutional structure"). Wang et al. [29] studied $LaSi_6$, $CeSi_6$, $YbSi_6$, and $LuSi_6$ with the Saunders "Kick" global stochastic method and found that the most stable structures were the substitutional structures. We reported that the most stable structures of $EuSi_n$, $SmSi_n$, and $YbSi_n$ ($n \leq 11$) are also substitutional structures [25–27]. Liu et al. [37] noted that the ground-state structures of $HoSi_n$ ($n = 1–12$, except for $n = 7$ and 10) were substitutional structures. In fact, the isomer reported by Liu et al. [37] (**7A** in Fig. 1) is less stable than the substitutional structure (**7B** in Fig. 1) by 0.15 and 0.17 eV when calculated at the B3LYP and PBE0 levels, respectively. For $HoSi_{10}$, when the isomer presented by Liu et al. [37] as the initial geometry (**10A** in Fig. 1) is optimized at the B3LYP level of theory, structure **10B** (shown in Fig. 1) is ultimately obtained. At the PBE0 level, structure **10B** in the 4A″ state is more stable than **10A** by 0.26 eV. Structure **10B**, similar to the most stable structure of $EuSi_{10}$ [25], can be viewed as that obtained by replacing a Si atom in the ground-state structure of Si_{11} [5] with a Ho atom. All of these results show that the most stable exohedral structures of neutral $RESi_n$ clusters can be viewed as the ground-state structure of Si_{n+1} with a Si atom swapped for an REM atom. Accordingly, only two families of initial geometries were taken into account in the optimization process in the work reported in the present paper: exohedral isomers (i.e., prolate structures that can be constructed by substituting a Si atom in the ground-state structure of Si_{n+1} with a Ho atom); and near-spherical geometries (obtained by a constrained search for structures similar to a fullerene cage). In order to find the most stable structures of $HoSi_n$ clusters as accurately as we could, previously reported ground-state structures of pure Si_n clusters [4, 6–9], especially those of TTP and SS type, were considered when constructing prolate $HoSi_n$ ($n = 12–20$) structures. Furthermore, the spin multiplicities of the quartet and sextuplet states were considered, noting that the electronic state is a quartet state if the 4*f* electrons of the Ho atom barely participate in bonding, while the electronic state is a sextuplet state if a 4*f* electron does participate in bonding. Although a large number of isomers were obtained, only a few selected isomers are presented in this paper.

Results and discussion

Lowest-energy structures and isomers

The isomers of the $HoSi_n$ ($n = 12–20$) clusters that were optimized with the PBE0 and B3LYP methods are shown in Fig. 2. The total and relative energies of the low-lying isomers are listed in Table 1.

There are three competing isomers for the ground-state structure of Si_{13}. At the CCSD(T)/6-31G(d)//MP2/6-31G(d) level, it is predicted to be a distorted TTP with an additional rhombus capping the edge of the prism [6]. At the quantum Monte Carlo level, it is predicted to be a C_{3v}-symmetry capped trigonal antiprism [4], and at the MP2/aug-cc-pVTZ//B3LYP/6-31+G(d) level, it is predicted to have C_{2v} symmetry [9]. The most stable structure, **12A**, of $HoSi_{12}$ can be viewed as a capped Si trigonal antiprism [4] with one of the Si atoms replaced with a Ho atom. Liu et al. [37] reported that the quartet-state isomer **12B** was the lowest-energy structure. Zhao et al. [38] noted that the semiclosed quartet-state isomer **12C** was the most stable structure. Energetically, the isomers **12B** (with quartet and sextuplet states) and **12C** (with a sextuplet state) are less stable than the quartet-state isomer **12A**.

For the isomer **12C** (quartet state), our result shows that spin contamination occurs due to the expectation value (4.75) of the total spin (S^2). This may be expanded in terms of pure states with higher multiplicities. On the other hand, the valence configuration ($6s^{0.44}4f^{10.04}5d^{2.45}6p^{0.78}$, as obtained at the B3LYP level) of the quartet state has five orbitals occupied by a single electron because of the transfer of one 4*f* electron. Energetically, both the quartet and sextuplet states are nearly identical, as can be seen from Table 1. These results indicate that the isomer **12C** is essentially in the sextuplet state. That is, the result of performing 4*f*-in-valence calculations is different from that produced by 4*f*-in-

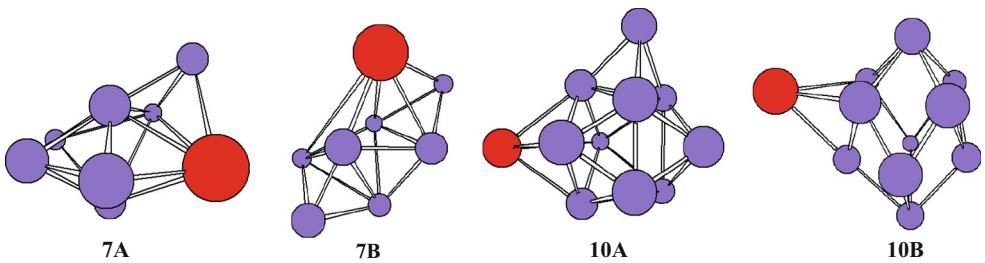

Fig. 1 Geometries of $HoSi_7$ and $HoSi_{10}$. Isomers **7A** and **10A** are taken from [37]. **7B** can be regarded as being derived from the ground-state structure of Si_8 [3] but with a Si atom replaced with a Ho atom.**10B** can be viewed as being derived from the ground-state structure of Si_{11} [5] but with a Si atom replaced with a Ho atom

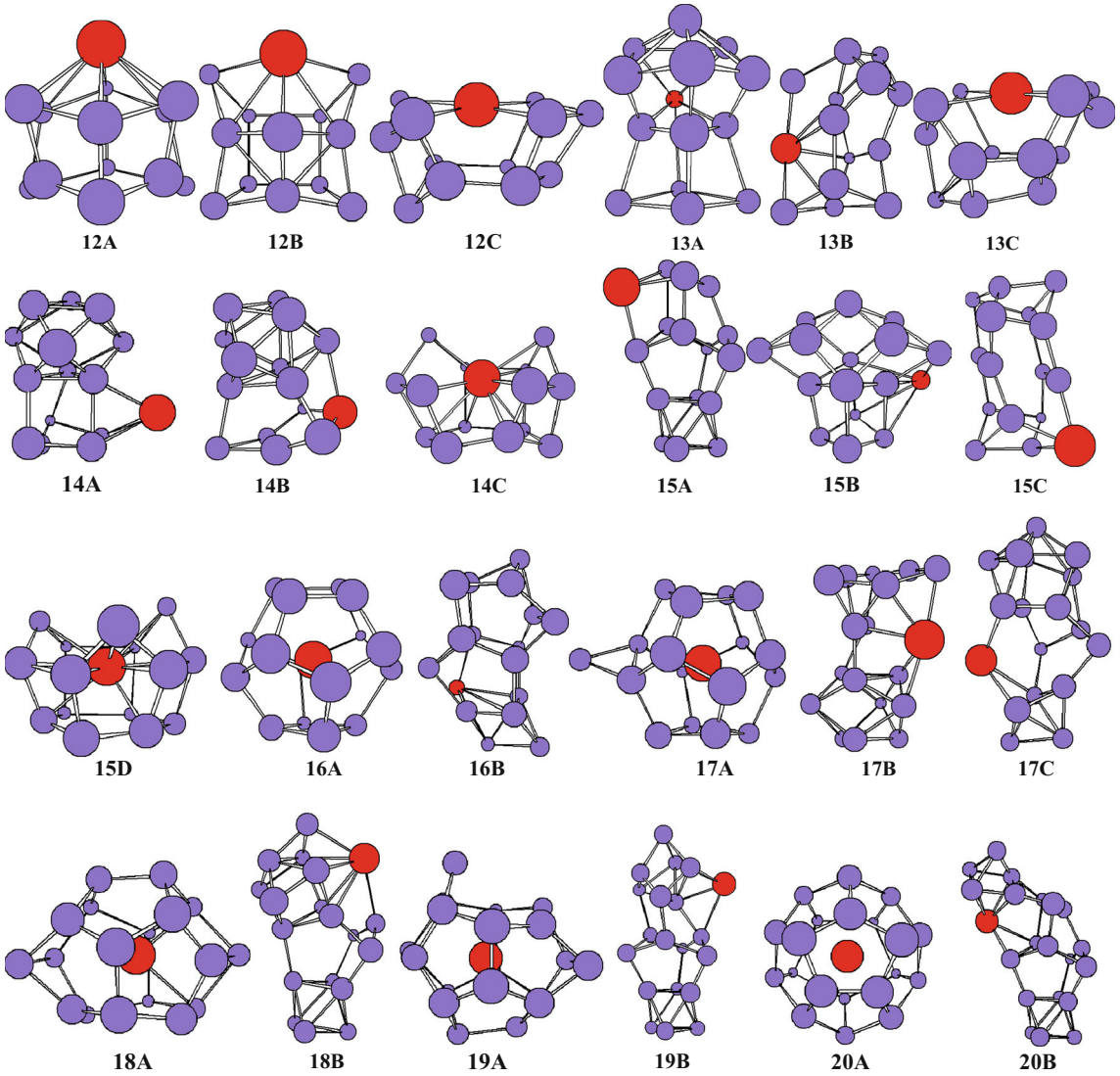

Fig. 2 The stable geometries of the isomers of the $HoSi_n$ ($n = 12$–20) clusters, as obtained at the B3LYP level of theory. The optimized geometries obtained at the PBE0 level of theory are similar to those yielded by B3LYP

core calculations. A similar situation is observed for the quartet-state isomers **13B**, **13C**, **14C**, **15D**, **16A**, **17A**, **18A**, **19A**, and **20A**; we do not delve any more deeply into this observation here.

The ground-state structure of Si_{14} is a face-capped distorted TTP with an additional rhombus capping an edge of the prism [6]. For $HoSi_{13}$, isomers **13A** and **13B** are constructed by replacing a Si in the ground-state Si_{14} [6] with a Ho atom. **13A** (quartet) is the global minimum. **13B** is the most stable when there is a sextuplet electronic state. Zhao et al. [38] reported that isomer **13C** was the most stable structure, but it is much higher in energy than the quartet-state **13A**.

The most stable structure of Si_{15} is a TTP with a tricapped trigonal antiprism [6]. Isomers **14A** and **14B** of $HoSi_{14}$ are constructed by replacing a Si in the most stable structure of Si_{15} [6] with a Ho atom. **14A** (quartet) was found to be the global minimum, and **14B** to be the most stable when there is a sextuplet electronic state. Isomer **14C** is taken from [38]. Isomer **14C** is considered to be higher in energy than the quartet-state isomer **14A**.

There are three competing isomers for the ground-state structure of Si_{16}; these contain a TTP motif, an SS motif, and two fused pentagonal prisms, respectively [7]. For $HoSi_{15}$, isomers **15A**, **15B**, and **15C** are constructed by substituting a Si in the most stable Si_{16} structure with a Ho atom. The structure of **15D**, with an incompletely encapsulated He atom, is taken from [39]. The sextuplet state of this isomer is less stable than the most stable (quartet-state) structure, **15A**, by about 0.83 and 1.03 eV when calculated at the B3LYP and PBE0 levels, respectively.

For $HoSi_{16}$, two isomers are reported. The prolate **16B** is constructed by substituting a Si in the ground-state structure of Si_{17} containing an SS motif [7] with a Ho atom. The

Table 1 Point group (PG), spin (S), S^2 operator, total energy (eV), and relative energy (ΔE, eV) of each isomer of each $HoSi_n$ ($n = 12$–20) cluster, as calculated at the B3LYP and the PBE0 levels of theory

Isomer	PG	S	B3LYP			PBE0		
			S^2	Total energy	ΔE	S^2	Total energy	ΔE
12A	C_1	3/2	3.76	−120343.03	0.00	3.76	−120297.90	0.00
	C_1	5/2	8.77	−120342.38	0.65	8.78	−120297.50	0.39
12B	C_1	3/2	3.78	−120342.54	0.50	3.78	−120297.38	0.52
	C_1	5/2	8.77	−120342.40	0.64	8.78	−120297.65	0.25
12C	C_s	3/2	4.75	−120341.69	1.34	4.78	−120296.40	1.50
	C_s	5/2	8.77	−120341.67	1.36	8.78	−120296.25	1.65
13A	C_s	3/2	3.76	−128220.97	0.00	3.76	−128172.86	0.00
	C_s	5/2	8.77	−128220.07	0.90	8.77	−128172.25	0.61
13B	C_1	3/2	4.72	−128220.48	0.49	4.76	−128172.39	0.47
	C_1	5/2	8.77	−128220.50	0.47	8.78	−128172.43	0.44
13C	C_1	3/2	4.79	−128219.91	1.06	4.81	−128171.37	1.50
	C_1	5/2	8.79	−128220.16	0.81	8.82	−128171.60	1.27
14A	C_1	3/2	3.76	−136098.53	0.00	3.76	−136047.12	0.00
	C_1	5/2	8.77	−136097.86	0.67	8.77	−136046.62	0.50
14B	C_s	3/2	3.76	−136098.24	0.29	3.76	−136046.56	0.56
	C_s	5/2	8.77	−136098.31	0.22	8.78	−136047.01	0.12
14C	C_1	3/2	4.80	−136097.67	0.86	4.85	−136045.41	1.71
	C_1	5/2	8.81	−136097.67	0.86	8.80	−136045.91	1.21
15A	C_s	3/2	3.77	−143976.87	0.00	3.76	−143921.52	0.00
	C_s	5/2	8.77	−143976.79	0.08	8.77	−143921.36	0.16
15B	C_1	3/2	3.76	−143976.37	0.50	3.76	−143921.47	0.05
	C_1	5/2	8.77	−143975.64	1.23	8.78	−143921.09	0.43
15C	C_1	3/2	3.76	−143976.35	0.52	3.76	−143920.91	0.61
	C_1	5/2	8.78	−143975.77	1.10	8.80	−143920.51	1.01
15D	C_1	3/2	4.78	−143976.03	0.84	4.79	−143920.56	0.96
	C_1	5/2	8.79	−143976.04	0.83	8.80	−143920.49	1.03
16A	C_s	3/2	4.78	−151854.92	0.05	4.78	−151796.34	0.16
	C_s	5/2	8.79	−151854.97	0.00	8.80	−151796.50	0.00
16B	C_1	3/2	3.76	−151854.95	0.02	3.77	−151796.18	0.32
	C_1	5/2	8.78	−151854.65	0.32	8.79	−151796.20	0.30
17A	C_1	3/2	4.78	−159732.77	0.12	4.79	−159670.88	0.01
	C_1	5/2	8.79	−159732.88	0.00	8.80	−159670.90	0.00
17B	C_1	3/2	3.76	−159732.67	0.21	3.77	−159670.83	0.07
	C_1	5/2	8.78	−159732.65	0.24	8.78	−159671.13	−0.23
17C	C_1	3/2	3.76	−159732.79	0.09	3.76	−159670.77	0.13
	C_1	5/2	8.77	−159732.14	0.75	8.77	−159670.44	0.46
18A	C_1	3/2	4.78	−167611.76	−0.01	4.80	−167546.42	−0.02
	C_1	5/2	8.78	−167611.75	0.00	8.79	−167546.40	0.00
18B	C_1	3/2	3.76	−167611.31	0.43	3.76	−167545.84	0.56
	C_1	5/2	8.77	−167610.60	1.14	8.77	−167545.44	0.96
19A	C_1	3/2	4.78	−175489.71	−0.02	4.80	−175420.84	−0.02
	C_1	5/2	8.78	−175489.69	0.00	8.79	−175420.82	0.00
19B	C_s	3/2	3.76	−175489.00	0.69	3.76	−175420.20	0.62
	C_s	5/2	8.77	−175488.46	1.23	8.78	−175419.82	0.99
20A	C_i	3/2	4.78	−183368.78	−0.02	4.80	−183296.37	−0.03
	C_i	5/2	8.78	−183368.76	0.00	8.79	−183296.34	0.00
20B	C_1	3/2	3.76	−183367.80	0.96	3.76	−183295.24	1.10
	C_1	5/2	8.77	−183367.28	1.48	8.77	−183295.03	1.31

endohedral isomer **16A** is taken from [39]. Its sextuplet state is more stable in energy than the quartet and sextuplet states of **16B** by 0.02 eV (B3LYP) or 0.32 eV (PBE0) and by 0.32 eV (B3LYP) or 0.30 eV (PBE0), respectively.

Isomers containing SS and TTP motifs compete to be the most stable structure of Si_{18} [7]. Isomers **17B** and **17C** of $HoSi_{17}$ are constructed by replacing an Si atom in the most stable Si_{18} structure with a Ho atom. The endohedral **17A** is almost the most stable of the structures, as reported previously [38]. Its sextuplet state is the ground-state structure at the B3LYP level, while it is less stable at the PBE0 level than the sextuplet-state isomer **17C** by 0.23 eV.

For $HoSi_{18}$, two isomers are identified. One is the prolate **18B**, which is constructed by replacing a Si in the most stable structure of Si_{19} (containing an SS motif) [7] with a Ho atom. Another is the endohedral **18A**, which is analogous to the most stable structure reported previously [38]. Its sextuplet state is predicted to be the ground state.

For $HoSi_{19}$, there are two isomers. The prolate **19B** is obtained by replacing a Si in the ground-state structure of Si_{20}

(containing an SS motif) [7] with a Ho atom. The cakelike **19A** is taken from [39]. Energetically speaking, its sextuplet state was calculated to be the most stable structure.

Two isomers are also reported for $HoSi_{20}$. The prolate **20B** is generated by replacing a Si in the most stable structure of Si_{21} (containing an SS motif) [8] with a Ho atom. The quartet and sextuplet states of isomer **20B** are much higher in energy than the sextuplet-state isomer **20A** with an encapsulated Ho when calculated at the B3LYP and PBE0 levels.

From the discussion above, we can conclude that, starting from $n = 16$, the sextuplet-state Si_n clusters with an encapsulated Ho atom are predicted to be the most stable structures (aside from when the isomers of $HoSi_{17}$ are calculated using the PBE0 method, when the most stable structure is found to be an exohedron in the sextuplet state). This small-core results obviously differ from the predictions obtained when using large-core basis sets for Ho atoms [38]. Although the geometries obtained are similar, their electronic states are different. The large-core results suggest that, when $n < 16$, exohedral quartet-state clusters are the ground states for $HoSi_n$. The quartet state for an endohedral and semiclosed geometry generally presents spin contamination. It is therefore crucial to inspect the spin contamination for clusters that include REM (and TM) atoms more closely.

Relative stabilities

To examine the relative stabilities of the most stable isomers of the $HoSi_n$ ($n = 12$–20) clusters, the binding energy per atom (BEPA) ($HoSi_n \rightarrow Ho + nSi$), where $BEPA(HoSi_n) = [nE(Si) + E(Ho) - E(HoSi_n)]/(n+1)$, was calculated at the B3LYP and the PBE0 levels for each isomer. A plot of BEPA against cluster size (Fig. 3) reveals that, when calculations are performed at the PBE0 level, the most stable isomers of $HoSi_{13}$, $HoSi_{16}$, $HoSi_{18}$, and $HoSi_{20}$ are slightly more stable than suggested by the smoothly increasing trend. In addition, the most stable isomer of $HoSi_{15}$ is also more stable when calculations are performed at the B3LYP level.

Apart from the BEPA, the dissociation energies (DEs) of the structures also illustrate their relative stabilities. DE1 [defined as the energy required for the disproportionation reaction $2HoSi_n \rightarrow HoSi_{n+1} + HoSi_{n-1}$, $DE1(HoSi_n) = E(HoSi_{n+1}) + E(HoSi_{n-1}) - 2E(HoSi_n)$] as a function of cluster size is shown in Fig. 4. From Fig. 4, we can see that $HoSi_{15}$, $HoSi_{17}$, and $HoSi_{19}$ are less stable than the other clusters because they are local minima at the PBE0 level, while $HoSi_{14}$, $HoSi_{17}$, and $HoSi_{19}$ are less stable than the other clusters when calculated at the B3LYP level.

Other measures of the cluster stability include $DE2(HoSi_n) = E(Si_n) + E(Ho) - E(HoSi_n)$, $DE3(HoSi_n) = E(HoSi_{n-1}) + E(Si) - E(HoSi_n)$, and $DE4(Si_n) = E(Si_{n-1}) + E(Si) - E(Si_n)$. The values of these parameters calculated at the B3LYP and the PBE0 levels of theory for the clusters of interest are sketched in Figs. 5 and 6, respectively. Analyses of the DE2 curve in Fig. 5 show that, at the B3LYP level, $HoSi_{13}$, $HoSi_{16}$, $HoSi_{18}$, and $HoSi_{20}$ are more stable than the clusters because their DE2 values are local maxima. $HoSi_{20}$ is the most stable of these clusters because it has the largest DE2 value. On the other hand, analyses of the DE3 and DE4 curves reveal that $HoSi_{13}$, $HoSi_{15}$, $HoSi_{16}$, $HoSi_{18}$, and $HoSi_{20}$ are more stable than the other clusters because their DE3 values are larger than their DE4 values. In other words, it is more energetically favorable to connect a Si atom to $HoSi_{n-1}$ to form $HoSi_n$ rather than to add it to Si_{n-1} to form Si_n. At the PBE0 level, the results of the analyses of DE2 are the same as those of the analyses of DE3 and DE4, and $HoSi_{13}$, $HoSi_{16}$, $HoSi_{18}$, and $HoSi_{20}$ are more stable than the other clusters.

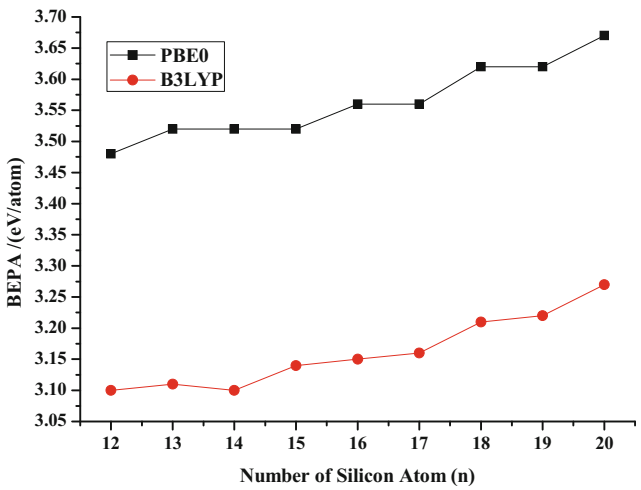

Fig. 3 Binding energy per atom (BEPA) for the most stable isomer of each $HoSi_n$ ($n = 12$–20) cluster, as calculated using the PBE0 and the B3LYP methods

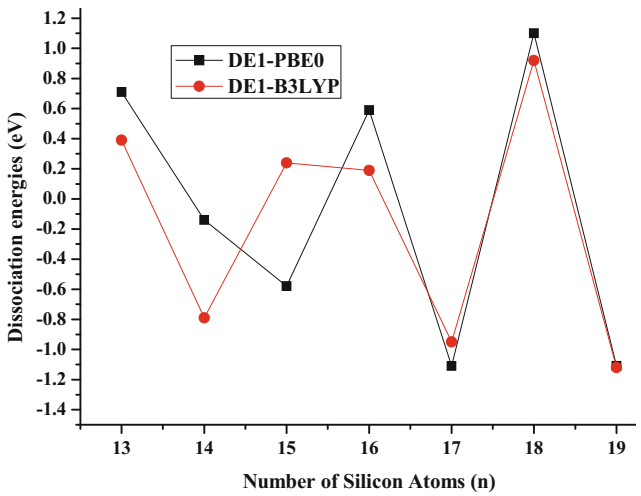

Fig. 4 DE1 (eV) of $HoSi_n$ ($n = 13$–19) versus the number of atoms n

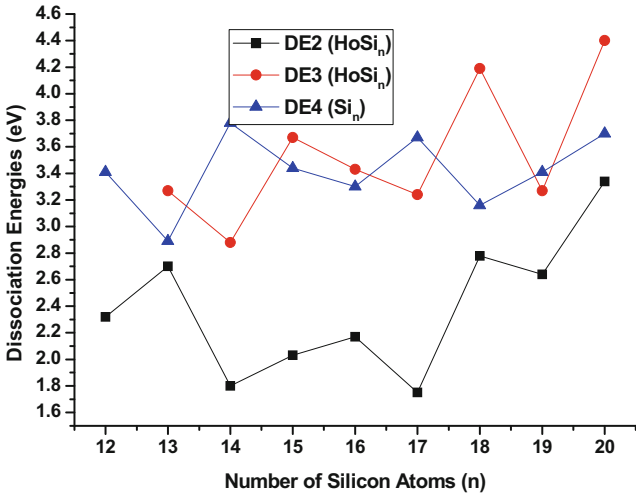

Fig. 5 DE2, DE3, and DE4 (eV) of the $HoSi_n$ (n = 12–20) clusters versus the number of Si atoms n, as calculated at the B3LYP level

From the discussion above, we can see that the relative stabilities of the clusters showed the same general trend regardless of the particular dissociation energy parameter used to judge the stability and the particular functional used to calculate the dissociation energy. $HoSi_{13}$, $HoSi_{16}$, $HoSi_{18}$, and $HoSi_{20}$ were found to be more stable than the other clusters. It should be noted that $HoSi_{16}$, $HoSi_{18}$, and $HoSi_{20}$ could be used as building blocks for nanomaterials because of their cage-like structures—especially $HoSi_{20}$, which is not only the most stable of these clusters but also features a Ho atom that is fully encapsulated in a Si_{20} fullerene-like framework.

Hardness

The hardness reflects the ability of a species to participate in a chemical reaction. The hardness—defined as the difference between the HOMO and the LUMO energies—of the most stable structure of each $HoSi_n$ (n = 12–20) cluster was evaluated at the PBE0 and the B3LYP levels, and the hardness values for all of the clusters of interest are sketched in Fig. 7. To facilitate comparison, the hardnesses of Si_n clusters are also shown in Fig. 7. From Fig. 7, we can see that the hardness curves obtained at the two levels of theory are very similar. Also, the hardness of each $HoSi_n$ (n = 12–20) cluster is smaller than that of its corresponding Si_n species except for $HoSi_{13}$ and $HoSi_{16}$; in other words, doping Ho into Si_{13} and Si_{16} results in clusters with good chemical stability. Accordingly, due to its particularly high chemical stability and relative stability, $HoSi_{16}$ may be viewed as a cluster that is especially appropriate for use as a building block for high-density magnetic storage nanomaterials (its magnetic moment is 5 μ_B; see the "Charge transfer and magnetic moment" section). Doping a Ho atom into Si_n (n = 12–20), with the exception of the n = 13 and 16 clusters, increases the photochemical sensitivity of the cluster. Therefore, given its high relative stability and photochemical sensitivity, the cluster $HoSi_{20}$, in which Ho is completely encapsulated by Si atoms, can be viewed as a particularly suitable building block for novel optical and optoelectronic photosensitive nanomaterials.

Note that, when using small-core basis sets, $HoSi_{16}$ does not have the largest predicted HOMO–LUMO gap among all of the clusters, in contrast to the result obtained when using large-core basis sets for the Ho atom [38].

Charge transfer and magnetic moment

Natural population analyses (NPA) of the ground-state structures were conducted using the PBE0 and B3LYP methods to further understand the interaction between the Ho atom and

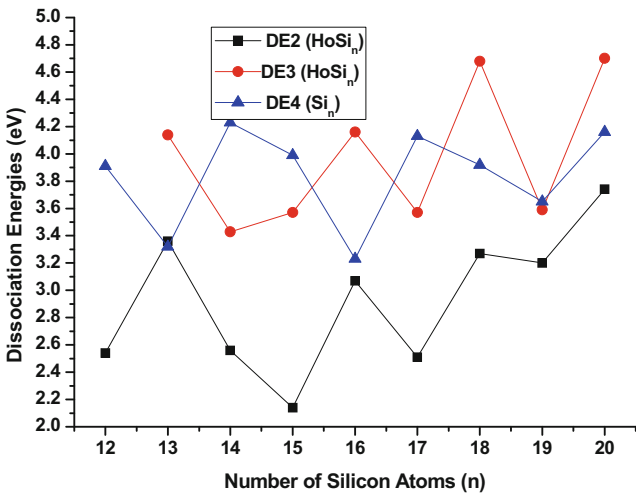

Fig. 6 DE2, DE3, and DE4 (eV) of the $HoSi_n$ (n = 12–20) clusters versus the number of Si atoms n, as calculated at the PBE0 level

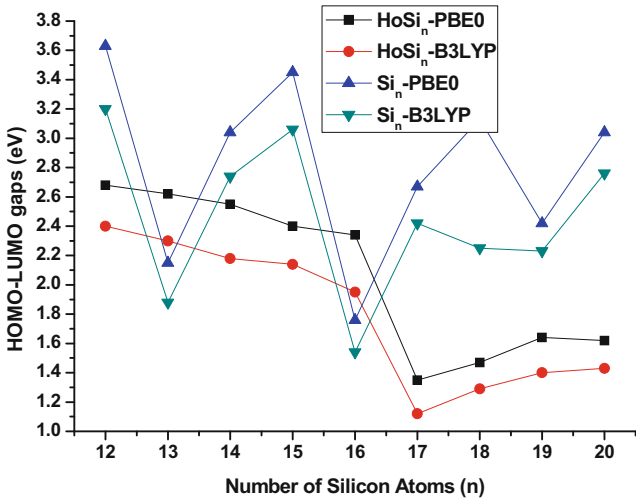

Fig. 7 The HOMO–LUMO gaps of the most stable structures of the clusters $HoSi_n$ and Si_n (n = 12–20), as calculated with the PBE0 and the B3LYP methods

Table 2 Natural population analysis (NPA), valence configuration, and charge on the Ho atom (in a.u.) as calculated at the B3LYP and the PBE0 levels for the lowest-energy isomer of each $HoSi_n$ (n = 12–20) cluster

Isomer	Method	Electron configuration	Charge (a.u.)
12A	B3LYP	[core]$6s^{0.15}4f^{10.97}5d^{0.86}6p^{0.23}6d^{0.01}$	0.81
	PBE0	[core]$6s^{0.14}4f^{10.97}5d^{0.87}6p^{0.25}6d^{0.01}$	0.79
13A	B3LYP	[core]$6s^{0.27}4f^{10.97}5d^{0.71}6p^{0.17}6d^{0.01}$	0.91
	PBE0	[core]$6s^{0.23}4f^{10.97}5d^{0.72}6p^{0.18}6d^{0.01}$	0.92
14A	B3LYP	[core]$6s^{0.21}4f^{10.97}5d^{0.63}6p^{0.12}6d^{0.01}$	1.10
	PBE0	[core]$6s^{0.15}4f^{10.98}5d^{0.64}6p^{0.13}6d^{0.01}$	1.13
15A	B3LYP	[core]$6s^{0.46}4f^{10.96}5d^{0.47}6p^{0.14}6d^{0.01}$	0.99
	PBE0	[core]$6s^{0.33}4f^{10.97}5d^{0.54}6p^{0.16}6d^{0.01}$	1.02
16A	B3LYP	[core]$6s^{0.40}4f^{10.00}5d^{4.72}6p^{1.67}6d^{0.07}$	−3.87
	PBE0	[core]$6s^{0.42}4f^{9.99}5d^{4.99}6p^{1.74}6d^{0.08}$	−4.23
17A	B3LYP	[core]$6s^{0.39}4f^{10.00}5d^{4.75}6p^{1.64}6d^{0.07}$	−3.83
	PBE0	[core]$6s^{0.40}4f^{9.99}5d^{5.03}6p^{1.70}6d^{0.07}$	−4.20
18A	B3LYP	[core]$6s^{0.36}4f^{10.01}5d^{4.25}6p^{1.53}6d^{0.06}$	−3.22
	PBE0	[core]$6s^{0.38}4f^{10.00}5d^{4.61}6p^{1.62}6d^{0.06}$	−3.68
19A	B3LYP	[core]$6s^{0.33}4f^{10.00}5d^{4.17}6p^{1.48}6d^{0.06}$	−3.03
	PBE0	[core]$6s^{0.36}4f^{10.00}5d^{4.48}6p^{1.58}6d^{0.06}$	−3.48
20A	B3LYP	[core]$6s^{0.27}4f^{10.01}5d^{3.95}6p^{1.41}6d^{0.05}$	−2.68
	PBE0	[core]$6s^{0.32}4f^{10.00}5d^{4.24}6p^{1.52}6d^{0.05}$	−3.14

the Si_n cluster. The charge on and the NPA valence configuration of the Ho atom in each cluster are listed in Table 2.

These data indicate that the charge on and NPA valence configuration of Ho calculated using the B3LYP method are usually the same as those obtained with the PBE0 method. The valence configurations of $6s^{0.15–0.46}4f^{10.96–10.98}5d^{0.47–0.87}6p^{0.12–0.25}$ for the most stable exohedral structures of the clusters $HoSi_n$ (n = 12–15) reveal that the 4*f* electrons are almost unchanged upon the creation of the $HoSi_n$ cluster and barely participate in bonding. However, for the most stable endohedral structures of the clusters $HoSi_n$ (n = 16–20), the valence configurations of $6s^{0.27–0.42}4f^{9.99–10.01}5d^{3.95–5.03}6p^{1.41–1.74}$ show that the 4*f* shell loses an electron during the creation of the $HoSi_n$ cluster; this electron is transferred to the 5*d* orbital and participates in bonding. In addition to the charge transfer from the 4*f* to the 5*d* orbital, charge transfer occurs from the 6*s* to the 5*d* and the 6*p* orbitals, leading to *spd* hybridization.

Table 2 also shows that charge is always transferred from the Ho atom to the Si_n cluster for exohedral $HoSi_n$ (n = 12–15) clusters, but the charge is transferred in the opposite direction for endohedral $HoSi_n$ (n = 16–20) clusters, which reveals that Ho acts as an electron acceptor in Si_n clusters in which Ho is fully encapsulated. In fact, the charge on the REM (or TM) atom in $REMSi_n$ clusters in which the REM atom is at the center of the Si_n cage is negative, and the smallest number of silicon atoms for $REMSi_n$ clusters with a negative charge on the REM atom is seen as the threshold value of n for the REM atom to be inserted into the silicon cage. The change transferred (2.68–4.23*e*) during the generation of the endohedral $HoSi_n$ (n = 16–20) clusters reveals that the bonding between the Ho and the Si_n cage is ionic, because the charge is transferred from the valence *sp* orbitals on silicon to the *spd* hybridized orbitals on Ho. Again, it should be noted that the small-core results for charge transfer are different from those predicted using large-core basis sets for the Ho atom: that the charge is always transferred from the Si atoms to the Ho atom in $HoSi_n$ (n = 12–20).

As far as species containing REM atoms are concerned, magnetism is one of their most interesting properties. The magnetic moments of the 6*s*, 4*f*, 5*d*, and 6*p* states for Ho, the total magnetic moment of Ho, and the total magnetic moment of the most stable structure of each $HoSi_n$ (n = 12–20) cluster are listed in Table 3. From the data shown, we can conclude that, for all of the clusters, the magnetic moments calculated using the B3LYP method are almost identical to those yielded by the PBE0 method. For each of the exohedral $HoSi_n$ (n = 12–15) clusters, the total magnetic moment is 3 μ_B, which comes from the 4*f* state (3.01–3.02 μ_B) of the Ho atom. For each of the endohedral $HoSi_n$ (n = 16–20) clusters, the magnetic moment is 5 μ_B, which derives mainly from the 4*f* state (3.98–3.99 μ_B) of Ho, followed by the 5*d* state (0.02–0.37 μ_B) and the 3*s* and 3*p* states (0.62–0.99 μ_B) of the Si atoms. There is no contribution from the 6*s* and 6*p* states of the Ho atom. In other words, for the endohedral structures of the $HoSi_n$ (n = 16–20) clusters, there is electron transfer from 4*f* to 5*d*. As a result, not only do the 4*f* electrons participate in bonding, but the total magnetic moment of each $HoSi_n$ (n = 16–20) cluster also increases.

Conclusions

The total energies, equilibrium geometries, relative stabilities, hardnesses, intramolecular charge transfer, and magnetic moments of the clusters $HoSi_n$ (n = 12–20) have been reexamined theoretically using the B3LYP and PBE0 functionals in combination with the cc-pVDZ basis set for the Si atoms and relativistic small-core Stuttgart effective core potentials (ECP28MWB) for the Ho atom. The results were obtained:

- When n = 12–15, the most stable structures of the $HoSi_n$ clusters are predicted to have exohedral geometries and a quartet ground state, and can be constructed by replacing a Si atom in the ground-state structure of Si_{n+1} with a Ho atom. However, the most stable structures were found to be endohedral frameworks with a sextuplet ground state when n = 16–20.
- Relative cluster stabilities were evaluated based on different dissociation energy parameters, which were calculated with the B3LYP and PBE0 functionals. Regardless of

Table 3 Magnetic moments (in μ_B) of the 6*s*, 4*f*, 5*d*, and 6*p* states of the Ho atom, the total magnetic moment (in μ_B) of the Ho atom, and the total magnetic moment of the ground-state structure of each $HoSi_n$ ($n = 12–20$) cluster, as calculated with the B3LYP and the PBE0 schemes

Isomer	Method	Magnetic moments of states of the Ho atom					Total magnetic moment of molecule
		6*s*	4*f*	5*d*	6*p*	Total	
12A	B3LYP	0.00	3.01	0.02	−0.04	2.99	3
	PBE0	0.00	3.01	0.02	0.01	3.04	3
13A	B3LYP	0.01	3.01	0.02	0.01	3.05	3
	PBE0	0.01	3.01	0.02	0.00	3.04	3
14A	B3LYP	0.01	3.01	0.02	0.00	3.04	3
	PBE0	0.00	3.01	0.02	0.00	3.03	3
15A	B3LYP	0.00	3.02	0.01	0.00	3.03	3
	PBE0	0.01	3.01	0.02	0.00	3.04	3
16A	B3LYP	0.00	3.99	0.36	0.01	4.36	5
	PBE0	0.00	3.99	0.37	0.02	4.38	5
17A	B3LYP	0.00	3.98	0.12	0.00	4.10	5
	PBE0	0.00	3.99	0.11	0.01	4.11	5
18A	B3LYP	0.00	3.99	0.10	0.01	4.10	5
	PBE0	0.00	3.99	0.09	0.00	4.08	5
19A	B3LYP	0.00	3.99	0.09	0.00	4.08	5
	PBE0	0.00	3.99	0.08	0.00	4.07	5
20A	B3LYP	0.00	3.99	0.05	0.00	4.04	5
	PBE0	0.00	3.99	0.02	0.00	4.01	5

the particular dissociation parameter considered, and the functional used to calculate it, the trend in relative stability across the clusters was the same. $HoSi_{13}$, $HoSi_{16}$, $HoSi_{18}$, and $HoSi_{20}$ were calculated to be more stable than the other clusters.

- In light of the results for cluster hardness, the most stable $HoSi_n$ clusters are achieved when a Ho atom is doped into Si_{13} and Si_{16} clusters. Doping Ho into the other Si_n clusters increases their photochemical sensitivity.
- Analyses of the intracluster charge transfer revealed that there is charge transfer from the Ho atom to the Si_n cluster when $HoSi_n$ ($n = 12–15$) clusters with exohedral structures are created. However, charge transfer occurs in the opposite direction when $HoSi_n$ ($n = 16–20$) clusters with endohedral structures are created. This shows that Ho acts as an electron acceptor when the Ho atom is encapsulated in the Si_n cage.
- Magnetic moment analysis of the clusters showed that the 4*f* electrons remain almost unchanged during the creation of the most stable exohedral structures of the $HoSi_n$ ($n = 12–15$) clusters, barely participating in the intracluster bonding. However, a 4*f* electron does participate in the bonding within the most stable endohedral frameworks of the $HoSi_n$ ($n = 16–20$) clusters; in these structures, a 4*f* electron is transferred to the 5*d* orbital, which hybridizes with the 6*s* and 6*p* orbitals and then interacts with the Si valence *sp* orbitals. Also, the total magnetic moments of the $HoSi_n$ ($n = 16–20$) clusters are considerably higher than those of the $HoSi_n$ ($n = 12–15$) clusters.

The results imply that, due to its especially high chemical stability and relative stability, the endohedral $HoSi_{16}$ cluster is particularly well suited for use as a building block in novel high-density magnetic storage nanomaterials. On the other hand, due to its prominent relative stability and photochemical sensitivity, the $HoSi_{20}$ cluster (in which Ho is completely encapsulated) appears to be a highly suitable building block for novel optical and optoelectronic photosensitive nanomaterials.

Acknowledgments This work was supported by the National Natural Science Foundation of China (grant no. 21263010), by the Program for Innovative Research Team in Universities of the Inner Mongolia Autonomous Region (grant no. NMGIRT-A1603), and by the Inner Mongolia Natural Science Foundation (grant no. 2015MS0216).

References

1. Raghavachari K (1986) J Chem Phys 84:5672–5686
2. Li BX, Cao PL, Zhan SC (2003) Phys Lett A 316:252–260
3. Vasiliev I, Öğüt S, Chelikowsky JR (1997) Phys Rev Lett 78:4805–4808
4. Grossman JC, Mitáš L (1995) Phys Rev Lett 74:1323–1326

5. Zhu X, Zeng XC (2003) J Chem Phys 118:3558–3570
6. Zhu X, Zeng XC, Lei YA, Pan B (2004) J Chem Phys 120:8985–8995
7. Yoo S, Zeng XC (2005) J Chem Phys 123:164303-1–164303-6
8. Yoo S, Zeng XC (2006) J Chem Phys 124:054304-1–054304-6
9. Nigam S, Majumder C, Kulshreshtha SK (2006) J Chem Phys 125: 074303-1–074303-11
10. Li S, Zee RJV, Weltner W Jr (1994) J Chem Phys 100:7079–7086
11. Xu CS, Taylor TR, Burton GR, Neumark DM (1998) J Chem Phys 108:1395–1406
12. Ohara M, Koyasu K, Nakajima A, Kaya K (2003) Chem Phys Lett 371:490–497
13. Honea EC, Ogura A, Peale DR, Félix C, Murray CA, Raghavachari K, Sprenger WO, Jarrold MF, Brown WL (1999) J Chem Phys 110: 12161–12171
14. Li S, Zee RJV, Weltner W Jr, Raghavachari K (1995) Chem Phys Lett 243:275–280
15. Koyasu K, Atobe J, Furuse S, Nakajima A (2008) J Chem Phys 129:214301-1–214301-7
16. Grubisic A, Ko YJ, Wang H, Bowen KH (2009) J Am Chem Soc 131:10783–10790
17. Li J, Wang G, Yao C, Mu Y, Wan J, Han M (2009) J Chem Phys 130:164514-1–164514-9
18. Zhao G, Sun J, Gu Y, Wang Y (2009) J Chem Phys 131:114312-1–114312-7
19. Peng Q, Shen J (2008) J Chem Phys 128:084711-1–084711-11
20. Liu T, Zhao G, Wang Y (2011) Phys Lett A 375:1120–1127
21. Dhaka K, Bandyopadhyay D (2015) RSC Adv 5:83004–83012
22. Li Y, Tam NM, Claes P, Woodham AP, Lyon JT, Ngan VT, Nguyen MT, Lievens P, Fielicke A, Janssens E (2014) J Chem Phys A 118: 8198–8203
23. Kenyon AJ (2005) Semicond Sci Technol 20:R65–R84
24. Ohara M, Miyajima K, Pramann A, Nakajima A, Kaya K (2002) J Chem Phys A 106:3702–3705
25. Yang JC, Wang J, Hao YR (2015) Theor Chem Accounts 134:81-1–81-11
26. Xie XH, Hao DS, Liu YM, Yang JC (2015) Comput Theor Chem 1074:1–8
27. Xie XH, Hao DS, Yang JC (2015) Chem Phys 461:11–19
28. Li CG, Pan LJ, Shao P, Ding LP, Feng HT, Luo DB, Liu B (2015) Theor Chem Accounts 134:34-1–34-11
29. Wang HQ, Li HF (2014) RSC Adv 4:29782–29793
30. Zhao RN, Han JG, Bai JT, Sheng LS (2010) Chem Phys 378:82–87
31. Zhao RN, Han JG, Bai JT, Liu FY, Sheng LS (2010) Chem Phys 372:89–95
32. Zhao RN, Ren ZY, Guo P, Bai JT, Zhang CH, Han JG (2006) J Phys Chem A 110(11):4071–4079
33. Cao TT, Zhao LX, Feng XJ, Lei YM, Luo YH (2009) J Mol Struct 895:148–155
34. Cao TT, Feng XJ, Zhao LX, Liang X, Lei YM, Luo YH (2008) Eur Phys J D 49:343–351
35. Kumar V, Singh AK, Kawazoe Y (2006) Phys Rev B 74:125411-1–125411-5
36. Wang J, Liu Y, Li YC (2010) Phys Chem Chem Phys 12:11428–11431
37. Liu TG, Zhang WQ, Li YL (2014) Front Phys 9:210–218
38. Zhao RN, Han JG (2014) RSC Adv 4:64410–64418
39. Adamo C, Barone V (1999) J Chem Phys 110:6158–6170
40. Becke AD (1993) J Chem Phys 98:5648–5652
41. Lee C, Yang W, Parr RG (1988) Phys Rev B 37:785–789
42. Woon DE, Dunning TH Jr (1993) J Chem Phys 98:1358–1371
43. Cao X, Dolg M (2002) J Mol Struct THEOCHEM 581:139–147
44. Frisch MJ, Trucks GW, Schlegel HB et al (2010) Gaussian 09, revision C.01. Gaussian Inc., Wallingford